ADVANCED HEALTHCARE MATERIALS
www.advhealthmat.de

Rapid Photocrosslinking of Silk Hydrogels with High Cell Density and Enhanced Shape Fidelity

Xiaolin Cui, Bram G. Soliman, Cesar R. Alcala-Orozco, Jun Li, Michelle A. M. Vis, Miguel Santos, Steven G. Wise, Riccardo Levato, Jos Malda, Tim B. F. Woodfield, Jelena Rnjak-Kovacina, and Khoon S. Lim**

Silk fibroin hydrogels crosslinked through di-tyrosine bonds are clear, elastomeric constructs with immense potential in regenerative medicine applications. In this study, demonstrated is a new visible light-mediated photoredox system for di-tyrosine bond formation in silk fibroin that overcomes major limitations of current conventional enzymatic-based crosslinking. This photomediated system rapidly crosslinks silk fibroin (<1 min), allowing encapsulation of cells at significantly higher cell densities (15 million cells mL^{-1}) while retaining high cell viability (>80%). The photocrosslinked silk hydrogels present more stable mechanical properties which do not undergo spontaneous transition to stiff, β-sheet-rich networks typically seen for enzymatically crosslinked systems. These hydrogels also support long-term culture of human articular chondrocytes, with excellent cartilage tissue formation. This system also facilitates the first demonstration of biofabrication of silk fibroin constructs in the absence of chemical modification of the protein structure or rheological additives. Cell-laden constructs with complex, ordered, graduated architectures, and high resolution (40 µm) are fabricated using the photocrosslinking system, which cannot be achieved using the enzymatic crosslinking system. Taken together, this work demonstrates the immense potential of a new crosslinking approach for fabrication of elastomeric silk hydrogels with applications in biofabrication and tissue regeneration.

1. Introduction

Silk fibroin is widely explored in biomedical[1] and high technology[2] applications due to the highly tuneable physico-chemical properties, of materials fabricated from this protein.[3] Silk fibroin has been bioengineered into a range of tissues toward regenerative medicine applications, and into 3D tissue models for testing pharmaceutical regiments and studying disease progression in vitro.[4] It is also extensively explored in drug delivery, soft electronics, and photonics applications.[2,5] The most extensively utilized silk fibroin is isolated from the domesticated *Bombyx mori* silkworm species, which has both a low inflammatory profile and cytotoxicity.[6] It is currently predominantly used in the clinic as a surgical suture and an absorbable surgical mesh.[1]

Hydrogels, highly hydrated polymer networks, can be fabricated from aqueous silk fibroin solutions using a variety of

Dr. X. Cui, B. G. Soliman, C. R. Alcala-Orozco, J. Li, M. A. M. Vis, Prof. T. B. F. Woodfield, Dr. K. S. Lim
Christchurch Regenerative Medicine and Tissue Engineering (CReaTE) Group
Department of Orthopaedics Surgery and Musculoskeletal Medicine
University of Otago
Christchurch 8011, New Zealand
E-mail: khoon.lim@otago.ac.nz

Dr. X. Cui, Prof. T. B. F. Woodfield, Dr. K. S. Lim
Medical Technologies Centre of Research Excellence
Auckland 1010, New Zealand

Dr. M. Santos, Dr. S. G. Wise
School of Medical Sciences
Department of Physiology
University of Sydney
Camperdown, NSW 2006, Australia

Dr. M. Santos, Dr. S. G. Wise
Charles Perkins Centre
University of Sydney
Camperdown, NSW 2006, Australia

Dr. R. Levato, Prof. J. Malda
Regenerative Medicine Center Utrecht
Heidelberglaan 100, 3584 CX Utrecht, The Netherlands

Dr. R. Levato, Prof. J. Malda
Department of Orthopaedics
University Medical Center Utrecht
Heidelberglaan 100, 3584 CX Utrecht, The Netherlands

Prof. J. Malda
Department of Equine Sciences
Faculty of Veterinary Medicine
Utrecht University
Domplein 29, 3512 JE Utrecht, The Netherlands

Prof. T. B. F. Woodfield, Dr. K. S. Lim
Maurice Wilkins Centre for Molecular Biodiscovery
Auckland 1010, New Zealand

Dr. J. Rnjak-Kovacina
Graduate School of Biomedical Engineering
University of New South Wales
Sydney 2052, Australia
E-mail: j.rnjak-kovacina@unsw.edu.au

The ORCID identification number(s) for the author(s) of this article can be found under https://doi.org/10.1002/adhm.201901667.

DOI: 10.1002/adhm.201901667

approaches, including sonication,[7] modulation of pH,[8] vortexing,[9] electrical stimulation,[10] and through addition of polar compounds, such as polyols or surfactants.[11] All these approaches rely on structural transformation of the fibroin protein chain from random coil to β-sheets. Hydrogen bonds are formed between the hydrophobic regions of the silk fibroin chains resulting in polymer chain re-arrangement and protein gelation.[3b] While this β-sheet transition allows hydrogel formation in the absence of chemical crosslinkers, the high stiffness and crystallinity associated with physically crosslinked silk fibroin hydrogels result in brittle, hard to handle materials that are not easily re-modeled by cells.[3b]

An alternative approach to fabricate silk fibroin hydrogels is via chemical crosslinking. While the fibroin polymer chain consists predominantly of nonreactive amino acids alanine and glycine, it does contain phenolic tyrosine residues (5.3%)[12] which can be catalyzed by horseradish peroxidase (HRP) and hydrogen peroxide (H_2O_2) to form di-tyrosine crosslinks.[4,3b,13a–d] This enzymatic (HRP/H_2O_2) crosslinking system has been previously used to fabricate silk fibroin hydrogels with high elasticity and tunable stiffness, which can be modulated through protein concentration, molecular weight, and solvent composition.[3b,14] However, the enzyme-catalyzed di-tyrosine crosslinking reaction requires long gelation times ranging between 15 min and 2 h.[3b,4] For cell encapsulation purposes, this might cause uneven cell distribution and leaves cells exposed to H_2O_2, which can result in cellular damage and low viability.[15] Moreover, these hydrogels undergo a spontaneous random coil to β-sheet transition, causing a gradual increase in hydrogel stiffness over time.[4] Unless specifically desired,[4] this 10–100-fold increase in stiffness over time makes the enzymatically crosslinked hydrogels unpredictable constructs for regenerative medicine applications.

Besides the enzymatic HRP/H_2O_2 reaction, other redox-based chemical reactions have been reported to facilitate di-tyrosine crosslinking, especially light-based systems involving photoinitiators such as riboflavin,[16] methylene blue,[17] and rose bengal.[18] In recent years, a visible light photoredox system using a combination of the transition metal complex, ruthenium (Ru), and a persulfate compound, has also been utilized to crosslink proteins into multiprotein complexes through the formation of di-tyrosine bonds.[19] During photoactivation, the photolysis of Ru^{2+} generates excited Ru^{3+} that in turn oxidize aromatic residues, such as tyrosine. These oxidized tyrosine groups are further converted into tyrosyl radicals, then subsequently quenched by forming di-tyrosine bonds with other nearby tyrosine groups. This specific photoredox reaction is not only efficient, but also very rapid, mainly due to the high absorbance of Ru in the visible light range and high chemical stability in the excited state. Tyrosine-rich proteins, including gelatin, fibrinogen, resilin, and silk, have been fabricated into hydrogels for regenerative medicine applications using this Ru-based photoredox reaction.[18,20] More recently, this visible light photoinitiated system has been employed toward 3D bioprinting, where gelatin-based bioinks were fabricated into complex architecture in a layer-by-layer fashion to mimic the physiological structures of native tissues.[21] The high efficiency and rapid reactivity of Ru allowed fabrication of scaffolds with high shape fidelity, minimal oxygen inhibition, and high resolution, using either extrusion-based or lithography-based bioprinting technologies.[21]

3D extrusion printing of silk fibroin has to date required addition of other compounds at high concentrations, including, e.g., gelatin (10–15 wt%),[22] glycerol (25 wt%),[23] or poly(ethylene glycol) (PEG, 40 wt%),[24] to achieve the necessary rheological properties for fiber extrusion. The crosslinking mechanisms utilized in these methods are not compatible with cell encapsulation at high densities required for most regenerative medicine applications. In one report of lithography-based 3D bioprinting of cell-laden silk fibroin constructs, the bioinks had to undergo a lengthy chemical modification process to introduce photolabile methacrylate groups onto the silk fibroin polymer chains.[25] To our knowledge, there are no studies to date on 3D biofabrication of non-chemically modified silk fibroin to fabricate constructs with high cell densities for regenerative medicine applications.

In this study, we present a rapid and cyto-compatible photocrosslinking process to produce cell-encapsulated silk hydrogels crosslinked through formation of di-tyrosine bonds. We demonstrate that hydrogels produced using this Ru-based photoredox reaction possess stable mechanical properties compared to hydrogels obtained through the HRP/H_2O_2 enzymatic reaction. We were able to combine the rapid photoredox reaction with advanced biofabrication technology to engineer constructs with complex and ordered architecture. A unique advantage of our approach is the ability to biofabricate complex constructs without chemically modifying the silk fibroin protein structure and composition or mixing with any rheological modifiers, which cannot be achieved using other alternative crosslinking mechanisms. To demonstrate the utility of this new biomaterial platform, we utilized it to bioengineer cartilage tissue in vitro. Articular chondrocytes were not only encapsulated within the hydrogel at high cell density, maintained long-term viability, but were also able to undergo very efficient chondrogenesis, making these promising constructs in cartilage tissue regeneration.

2. Experimental Section

Lithium bromide, ITS, L-proline, L-ascorbic acid-2-phosphate sesquimagnesium salt (AsAp), dexamethasone, fast green, sodium azide, hyaluronidase, sodium chloride, 1,9-dimethylmethylene blue zinc chloride double salt (DMMB), proteinase K, protease type XIV, *tris*(2,2-bipyridyl)dichlororuthenium(II) hexahydrate (Ru), sodium persulfate (SPS), calcein-AM, propidium iodide, phosphate buffered saline (PBS), horseradish peroxidase type VI (HRP), hydrogen peroxide (H_2O_2), Corining cell strainer (size 100 μm), Pluronic F-127, and cellulose dialysis membrane (14 kDa molecular weight cutoff) were purchased from Sigma-Aldrich, St Louis, MO. Dulbecco's modified Eagle's medium (DMEM) high glucose, 4-(2-hydroxyethyl)-1-piperazine-ethanesulfonic acid (HEPES), fetal calf serum, 0.25% trypsin/EDTA (ethylenediaminetetraacetic acid), nonessential amino acids (NEAA), fetal bovine serum (FBS), CyQuant cell proliferation assay kit, AlamarBlue, Trypsin-EDTA solution, SYBRTM Green PCR Master Mix, Trizol, and penicillin streptomysin (PS) were purchased from Thermo Fisher Scientific,

Auckland, New Zealand. Primary antibody against collagen II (II-II6B3-C) was purchased from DSHB, Iowa City, USA. Primary antibodies against collagen I (ab34710) and aggrecan (ab3773) were acquired from Abcam, Melbourne, Australia. Transforming growth factor β-1 (TGF-β1) was obtained from R&D systems, Minneapolis, USA. Type II collagenase was purchased from Worthington biochemical corporation, Lakewood, USA. VectorDAB, ImmPACTTM VIP, ImmPACTTM AEC, and VECTASTAIN ELITEABC Kits (Peroxidase) were purchased from Vector Laboratories, Burlingame, USA. Optimal cutting temperature (OCT) compounds were purchased from Leica Biosystems, Wetzlar, Germany.

2.1. Isolation of Silk Fibroin

Silk fibroin solution was isolated from *Bombyx mori* silkworm cocoons as previously described.[26] Cocoons (Tajima Shoji, Japan) were cut into small pieces and boiled in 0.02 M sodium carbonate solution (5 g cocoons per 2 L of Na_2CO_3) for 5 min or 30 min in a degumming process designed to remove sericin from the silk fibroin fiber. Boiling time was correlated with silk molecular weight, as previously described[27] The degummed silk fibroin fibers were dissolved in lithium bromide (9.3 M) at 20 wt% for 2–4 h at 60 °C until fully dissolved. The silk fibroin solution was dialyzed against deionized water using a cellulose membrane (14 kDa cut-off) for 5 days with daily water changes. 200 µL silk solution was freeze-dried and weighted to obtain silk concentration in wt%. The solution was stored at 4 °C until required.

2.2. Fabrication of Silk Fibroin Hydrogels Using Photocrosslinking or Enzymatic Crosslinking

Silk fibroin hydrogels of different formulations were prepared as detailed in **Table 1**. Gelatin (0.5 wt%) was incorporated to support cell interactions. 50 µL of each hydrogel solution was pipetted into a silicon mold (5.5 mm diameter and 2 mm height). For visible light crosslinking, samples were irradiated with 30 mW cm^{-2} visible light for 3 min (400–450 nm, Rosco IR/UV filter equipped to OminiCure S1500). For enzymatic crosslinking, samples were crosslinked at 37 °C for 1.5 h as previously described.[3b]

Table 1. Silk fibroin (SF) hydrogel formulations fabricated using the photocrosslinking or enzymatic crosslinking method.

Crosslinking mechanism	Name	Silk fibroin [wt%]	Gelatin [wt%]	Degumming time [min]
Photocrosslinking 0.5×10^{-3} M Ru 5×10^{-3} M SPS	SF-P5	2	–	5
	SF-P5G	2	0.5	5
	SF-P30	2	–	30
	SF-P30G	2	0.5	30
Enzymatic crosslinking 10 U mL^{-1} HRP 3.3×10^{-3} M H_2O_2	SF-E5	2	–	5
	SF-E5G	2	0.5	5
	SF-E30	2	–	30
	SF-E30G	2	0.5	30

2.3. Mass Loss and Swelling Ratio

The initial weight (m_{iw}) of silk fibroin hydrogel constructs was recorded after the crosslinking. Three samples from each conditions were immediately (t = 0) freeze-dried, and the corresponding dried weight was recorded (m_{id}). The macromer fraction (M%) was calculated using Equation (1) below

$$M\% = m_{id}/m_{iw} \quad (1)$$

The remaining samples from each condition were incubated in cell culture medium at 37 °C. After 1 day (t = 24 h), the swollen weight of the samples was recorded (m_s), followed by freeze-drying to obtain the final dried weight (m_d). The sol fraction value which was defined as polymer chains not crosslinked into the network was calculated using Equation (2). The mass swelling ratio (q) was calculated using Equation (3)

$$\text{Sol fraction} = 100\% \times (m_{id} - m_d)/m_{id} \quad (2)$$

$$\text{Swelling ratio } q = m_s/m_d \quad (3)$$

2.4. Mechanical Testing

Young's modulus was determined from the linear region of the stress–strain curves (10–15% strain) obtained using an MTS Criterion42 mechanical testing machine equipped with a 5 N load cell. Cylindrical samples (height = 2 mm, diameter = 5.5 mm) were incubated in cell culture media for different periods of time (day 1, weeks 1, 2, 3, 4, 5) prior to compression testing. During the measurement, samples were loaded parallel to their long axis and compressed at a constant crosshead speed at 0.01 mm s^{-1}. All measurements were performed at ambient temperature with a preload setting of 0.1 N.

2.5. Quantification of β-Sheet Using FTIR-ATR

β-sheet crystallinity was determined by Fourier transform spectroscopy in attenuated total reflectance mode (FTIR-ATR) using a Bruker Alpha spectrometer (MA, USA). Infrared spectra were collected by averaging a total of 64 scans at a spectral resolution of 4 cm^{-1} within the wavenumber range of 500–4500 cm^{-1}. Amide I bands (1585–1710 cm^{-1}) were deconvoluted using a Fourier self-deconvolution (FSD) algorithm by adopting Gaussian line profiles. The relative contribution of each secondary structure was determined by integration of the corresponding fitted peaks obtained from FSD calculations. The position of each peak was further confirmed by double differentiation of the amide I envelopes and peak assignment was as follow:[28] side chains (1595–1605 cm^{-1}); β-sheets (1610–1628 and 1697–1704 cm^{-1}); random coils (1635–1650 cm^{-1}); alpha-helix (1652–1660 cm^{-1}), and beta-turns (1663–1695 cm^{-1}). A nonlinear least-square

convergence criterion monitored the error between the original and deconvoluted spectra, imposing relative errors below 10^{-6}. The contribution of β-sheets was determined by calculating the relative areas of the corresponding peaks in the area-normalized deconvoluted amide I profile.

2.6. Cell Isolation, Culture, and Encapsulation

Human articular chondrocytes (HACs) were isolated from macroscopically normal regions of articular cartilage from human patients undergoing anterior cruciate ligament reconstruction. Patient's consent was obtained prior to tissue collection under approved ethics from the institutional ethical committee (Health and Disability Ethics Committee New Zealand, URB/07/04/014/AM09). The harvested cartilage tissues were digested using 0.15% Type II collagenase in chondrogenic expansion media (DMEM with 0.4×10^{-3} M L-proline, 10×10^{-3} M HEPES, 0.1×10^{-3} M NEAA, 100 U mL^{-1} penicillin, 0.1 mg mL^{-1} streptomycin, 0.1×10^{-3} M AsAp, and 10% FBS) at 37 °C for 16–20 h in a 5% CO_2 and humidified atmosphere incubator. The digested cartilage tissue was filtered through a cell strainer (100 µm), and the isolated cells were cultured in chondrogenic expansion media at 5 25 000 cells cm^{-2} and passaged three times (P1–P3).

For cell encapsulation experiments, HACs were first mixed with silk fibroin hydrogel solutions at cell densities ranging from 2.5 to 15 million cells mL^{-1}. The hydrogel precursor solutions consisted of cells and silk fibroin mixtures indicated in Table 1, were crosslinked as described in Section 2.2. All formulations were supplemented with 0.9 g L^{-1} NaCl to provide an isotonic environment during cell encapsulation process. The cross-linked cell-laden constructs were incubated in 400 µL chondrogenic differentiation medium (DMEM with 0.4×10^{-3} M L-proline, 10×10^{-3} M HEPES, 0.1×10^{-3} M NEAA, 100 U mL^{-1} penicillin, 0.1 mg mL^{-1} streptomycin, 0.2×10^{-3} M AsAp, 1 × ITS+1 premix, 1.25 mg mL^{-1} BSA, 10×10^{-9} M dexamethasone, and 10 ng mL-1 TGFβ-1). For long-term cell culture experiments, all samples had 15 million cells mL^{-1}, and were cultured for up to 5 weeks. Cell-free silk hydrogels were also prepared and cultured as negative controls. HAC microtissues/aggregates (1 mm diameter) were used as positive control and prepared as previously described.[29] Briefly, cells were seeded in a v-bottom 96-well plate at a concentration of 2 50 000 cells per well. Plates were then centrifuged at 200 *g* for 4 min, to allow cellular aggregation, then cultured at 37 °C in a humidified air incubator (5% CO_2/95% air) for 5 weeks in chondrogenic differentiation media, refreshed twice a week.

2.7. Cell Viability and Metabolic Activity

Live/dead assay was performed using 1 µg mL^{-1} of calcein-AM and propidium iodide (live/dead stain, respectively) at day 1 and day 35. Briefly, cell-laden hydrogel constructs were washed three times with PBS and incubated for 20 min incubation in the dye solution at 37 °C. Constructs were washed with PBS three times and imaged using a fluorescent microscope (Axio Observer Z1 inverted microscope, Carl Zeiss, Germany). Images were processed using ImageJ to count the number of live and dead cells. Cell viability was calculated using Equation (4)

$$\text{Cell viability} = \frac{\text{Number of live cells}}{\text{Number of (Live cells + dead cells)}} \times 100\% \quad (4)$$

AlamarBlue assay was used to analyze and track the metabolic activity of encapsulated HAC in silk fibroin hydrogels. Briefly, at days 1, 7, 14, 21, 28, and 35 post-encapsulation, 400 µL of 10 v/v% AlamarBlue reagent in DMEM was added into each cell culture well and incubated for 1 h at 37 °C. 100 µL of the Alamar blue solution was taken from each well (four samples per well) and the absorbance was recorded (Thermo Scientific Varioskan TM Flash, Auckland, New Zealand) at 570 and 600 nm. Dye reduction rate was calculated according to manufacturer's instructions.

2.8. Quantification of Tissue Formation Using Glycosaminoglycan (GAG) and DNA Assays

Total DNA and GAG content was quantified in cell-laden hydrogels at day 1, day 7, day 21, and day 35 post-cell encapsulation. Samples were washed three times with PBS, freeze-dried, and weighted. The dried samples were digested in a cocktail consisting of 500 µg mL^{-1} protease XIV and 1 mg mL^{-1} proteinase K dissolved in 10×10^{-3} M Tris-HCl and 1×10^{-3} M disodium EDTA solution at 56 °C until fully dissolved. For DNA quantification, samples were treated with 1.35 U mL^{-1} RNase for 1 h at room temperature prior to quantifying total DNA content using the CyQUANT Cell Proliferation Assay Kit. Total GAG content was quantified using the dimethylmethylene blue (DMMB) assay as previously described.[29]

2.9. Gene Expression

The expressions of chondrogenic genes was evaluated using quantitative polymerase chain reaction. Samples were collected at day 1, day 7, and day 35 post-cell encapsulation and fragmented by mechanical stirring in 1 mL Trizol reagent for 30 min at room temperature and RNA was isolated using according to manufacturer's instruction. Expression of collagen I, collagen II, collagen X, aggrecan, and Sox-9 was measured using the LightCycler 480 system (Roche Diagnostics, Auckland, New Zealand) and SYBR Green I MasterMix. Glyceraldehyde 3-phosphate dehydrogenase (GAPDH) was used as the housekeeping gene to calculate gene expression using the $\Delta\Delta C_t$ method. Primer sequences are included in Table S2 in the Supporting Information. The fold change in gene expression was normalized to the cells at day 0 before encapsulation in hydrogels or pellet culture.

2.10. Histology and Immunohistochemistry

Cell-laden silk hydrogels were collected at day 35 post-cell encapsulation, fixed with 4% neutral buffered formalin for 1 h

before infiltrating with OCT compound at 4 °C overnight and incubated at –80 °C for 30 min. The frozen samples were cryosectioned into 30 µm thick sections. Hematoxylin and Safranin-O were used to stain cell nuclei and GAGs, respectively. Samples were imaged using a bright field light microscope (Axio Observer Z1 inverted microscope, Carl Zeiss, Germany). For immunohistochemistry, tissue sections were soaked in 0.1 wt% hyaluronidase in PBS for 30 min at 37 °C then blocked with a solution of 2 wt% BSA with 0.3 M glycine at room temperature for 30 min. Samples were incubated in 0.3 wt% H_2O_2 in tap water for 30 min to quench endogenous peroxide activities followed by three washed in PBS. Sections were incubated with primary antibodies against collagen I (1:200), collagen II (1:200), or aggrecan (1:300) in 2 wt% BSA solution at 4 °C overnight. Samples were washed three times with blocking buffer and incubated with VECTASTAIN ABC agent for 30 min followed by another 5 min wash in blocking buffer. The substrate solution (Vector DAB for collagen I and aggrecan and ImmPACT VIP for collagen II) was added and samples were incubated at room temperature until the desired stain intensity developed. Samples were washed with tap water and imaged as described above. Cell-free silk hydrogels were used as negative controls to identify background and nonspecific staining. HAC microtissues are used as positive controls.

2.11. 3D Biofabrication of Silk Fibroin Hydrogels

The poloxamer Pluronic F-127[30] (30 wt%) was extruded through a needle at a temperature of 25 °C using a BioScaffolder (SYS+ENG, Germany) and deposited onto a 30 °C plate to facilitate stabilization of the sacrificial template. For simple designs, Pluronic F-127 filaments were deposited in a layer-by-layer 0°–90° orientation with varying filament spacing of 1 mm and varying fiber diameter of 0.5, 0.75, or 1 mm by varying the print head XYZ-plane speed, spindle motor speed, and needle size (**Table 2**). For more complex designs, Pluronic F-127 filaments of 0.5 mm were deposited in a 0°–45° to 135°–90° orientation, varying filament spacing between 0.1, 0.2, and 0.5 mm. The specific Pluronic F-127 sacrificial template design and the continuous double extrusion-printing process are demonstrated in the Supporting Information (Figures S1–S3, Supporting Information). Silk solution was further extruded into the Pluronic F-127 template at a spindle motor speed of 8 mm min^{-1}, using a 21G needle (0.6 mm inner diameter), to allow the non-viscous silk solution to infiltrate the porous Pluronic F-127 sacrificial templates simply through capillary motion. Thereafter, the silk-infiltrated Pluronic F-127 constructs were subjected to photocrosslinking, using conditions as outlined in Section 2.2. The photocrosslinked constructs were then incubated in 4 °C PBS for 3 min to remove the Pluronic F-127 sacrificial template.

Table 2. Settings for 3D extrusion printing of Pluronic F-127 sacrificial scaffolds.

Fiber diameter [mm]	Fiber spacing [mm]	Needle inner diameter [mm]	Print head speed [mm min^{-1}]	Spindle motor speed [mm min^{-1}]
0.5	1	0.3 (23G)	700	8
0.75	1	0.6 (21G)	500	9
1	1	0.9 (19G)	300	13

2.12. Statistical Analysis

Data are expressed as mean ± standard deviation. All results were analyzed using one- or two-way analysis of variance (ANOVA) with Bonferroni's multiple comparisons post hoc tests unless stated otherwise. The models were constructed using Prism (GraphPad Software, Version 7). Samples in each study were prepared in triplicate ($N = 3$), and all studies were repeated at least three times ($N = 3$) for a total of nine samples. Statistical significance was accepted at $p < 0.05$.

3. Results

Silk fibroin of high (5 min degumming) and low (30 min degumming) molecular weight was crosslinked either via enzymatic (HRP/H_2O_2) or photocrosslinking (Ru/SPS and visible light) mechanisms, targeting tyrosine moieties (**Figure 1**). The effect of the molecular weight and reaction mechanism on the

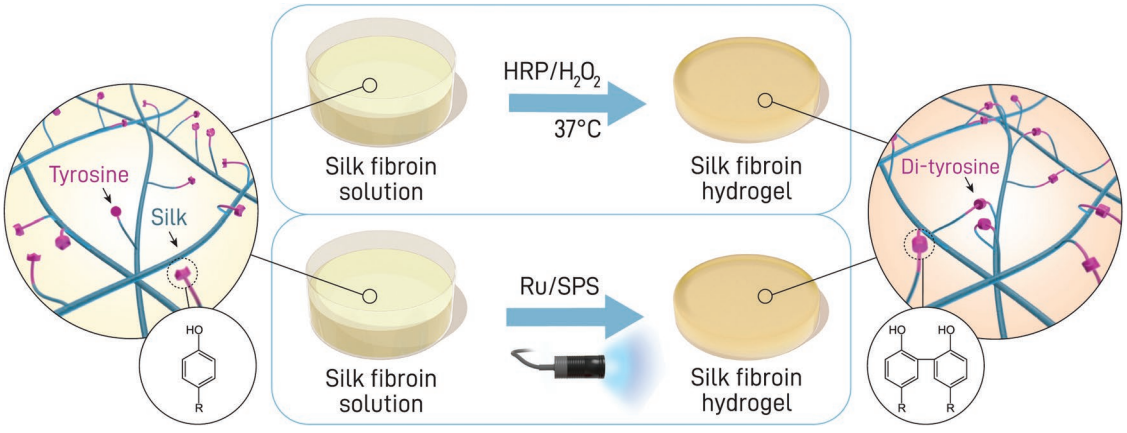

Figure 1. Schematic of enzymatic (HRP/H_2O_2) crosslinking and visible light photocrosslinking (Ru/SPS) mechanism to fabricate silk fibroin hydrogels through di-tyrosine bonds formation.

crosslinking efficiency, mechanical properties, and interaction with human primary articular chondrocytes was studied over time. Each condition was tested in the presence or absence of gelatin, utilized to improve cellular interactions with silk.

3.1. Physico-Chemical and Mechanical Properties of Enzymatically or Visible Light Photocrosslinked Silk Hydrogels

Regardless of the silk molecular weight, there was no significant difference in the sol fraction values (**Figure 2**A) or swelling ratio (Figure 2B) between the two crosslinking mechanisms. Incorporation of gelatin did not negatively impact the photocrosslinking efficiency, as demonstrated by no change in the sol fraction values and mass swelling ratio (Figure 2C,D). Similarly, enzymatically crosslinked hydrogels with or without gelatin had similar sol fraction values and mass swelling ratios (Figure S4, Supporting Information), suggesting that the presence of gelatin did not impair the di-tyrosine crosslinking reaction. Furthermore, photorheological data showed that the photocrosslinking reaction is very rapid where 5 s of light irradiation was sufficient to facilitate the sol–gel transition (Figure S5, Supporting Information).

Enzymatically crosslinked silk hydrogels have been previously shown to undergo a drastic change in mechanical properties over time, when incubated in PBS or cell culture media, attributed to the formation of beta-sheets.[15] Unconfined compressive modulus of silk fibroin hydrogels generated via photocrosslinking was therefore compared to those fabricated via enzymatic crosslinking over a period of 5 weeks in cell culture media at 37 °C. The compressive modulus of all fabricated silk hydrogels after equilibrium swelling (1 day post crosslinking) were measured to be not significantly different (18–24 kPa, $p > 0.05$) regardless of the molecular weight and crosslinking mechanism. However, the compressive modulus of enzymatically crosslinked silk hydrogels changed significantly after 2 weeks ($p < 0.0001$) for both SF-E5 and SF-E30 (Figure 2E,F), reaching a final modulus of 166 ± 15.0 kPa (SF-E5) and 197.5 ± 8.1 kPa (SF-E30) at 5 weeks, a fold change of 9.3 and 8.3, respectively. In contrast, the compressive modulus of photocrosslinked silk hydrogels remained stable, with no significant changes over the 5 week period. The addition of gelatin had no impact on the mechanical properties of photocrosslinked silk hydrogels (Figure 2G,H). The presence of gelatin in enzymatically crosslinked silk hydrogels did not prevent the structural change leading to the shift in compressive modulus, but it did reduce the overall modulus from week 2 onward (Figure S4, Supporting Information).

In order to further understand the observed difference in mechanical properties of the silk hydrogels fabricated using enzymatic and photocrosslinking systems, the β-sheet crystallinity of silk fibroin hydrogels fabricated from low molecular weight silk was analyzed using FTIR-ATR.[31] The representative Amide I and corresponding Fourier self-deconvoluted peaks used for beta-sheet crystallinity calculation were shown in Figure S6 in the Supporting Information. The initial β-sheet crystallinity (1 day after crosslinking) was similar for both SF-E30 (30.7 ± 3.3%) and SF-P30 (30.8 ± 1.4%) (Figure 2I). Interestingly, the overall β-sheet content of SF-E30 increased gradually over time and was significantly higher after 35 days of incubation compared to day 1 (42.7 ± 2.7%, $p = 0.0004$). In contrast, although SF-P30 had a slight increase in β-sheet crystallinity to 36.9% ± 2.7% after 35 days, this increment was not statistically significant compared to day 1 ($p = 0.08$).

3.2. High Density Cell Encapsulation in Photocrosslinked Silk Fibroin Hydrogels

Cell encapsulation studies were performed using primary HACs embedded in silk hydrogels crosslinked using either enzymatic or photocrosslinking mechanisms. Silk fibroin solutions containing more than 2.5 million cells mL^{-1} did not crosslink nor form stable hydrogels when enzymatically crosslinked (**Figure 3**A). In contrast, photomediated crosslinking supported fabrication of HAC-laden hydrogels with cell densities up to 15 million cells mL^{-1}, with high structural stability and ease of handling. Therefore, all long-term cell-culture experiments were only conducted with photocrosslinked silk hydrogels using a cell density of 15 million cells mL^{-1}, where cell viability, metabolic activity, and proliferation were measured over a 5 week culture period. Reduction of AlamarBlue reagent was used to assess cell metabolic activity, with higher reduction rates indicating higher cellular metabolic activity. There were no major changes in the overall cell metabolic activity over time (Figure 3B). Addition of gelatin significantly improved cell metabolic activity as observed in SF-P5G and SF-P30G compared to their respective counterparts (SF-P5 and SF-P30) ($p < 0.05$), at all time-points except at 5 weeks post-encapsulation (Figure 3B). DNA/dry weight ratio was used as an indicator of cell proliferation. All conditions had a similar initial value at around 1 µg DNA per mg of dry hydrogel (Figure 3C). After 5 weeks of culture, all conditions showed significantly ($p < 0.05$) higher DNA content (1.6-fold increase on average), with no statistically significant differences in DNA content between any conditions. Live/dead cell staining was performed at 1 day or 5 weeks post-encapsulation to assess the viability of cells encapsulated in photocrosslinked hydrogels (Figure 3D,E). At day 1, both SF-P5 and SF-P30 showed relatively low cell viability at 52.0 ± 8.5% and 44.7 ± 9.5%, respectively. The cell viability was significantly improved in the presence of gelatin, at 73.5 ± 7.0% (SF-P5G, $p < 0.05$) and 73.5 ± 9.7% (SF-P30G, $p < 0.01$). Although the cell viability increased in all conditions at 5 weeks relative to day 1, statistical difference was only observed in the SF-P30 constructs (Figure 3E, $p < 0.01$). There were no significant differences in cell viability between any of the conditions at week 5, with relatively high viability of 68–83% (Figure 3E).

3.3. Cartilage Tissue Formation in Photocrosslinked Silk Fibroin Hydrogels

HACs encapsulated in photocrosslinked silk fibroin hydrogels were able to remodel their microenvironment, secreting extracellular matrix (ECM) over time and increasing the compressive modulus of the hydrogel constructs. The compressive modulus of all cell-laden hydrogels increased over the 5 week culture period regardless of the molecular weight or presence

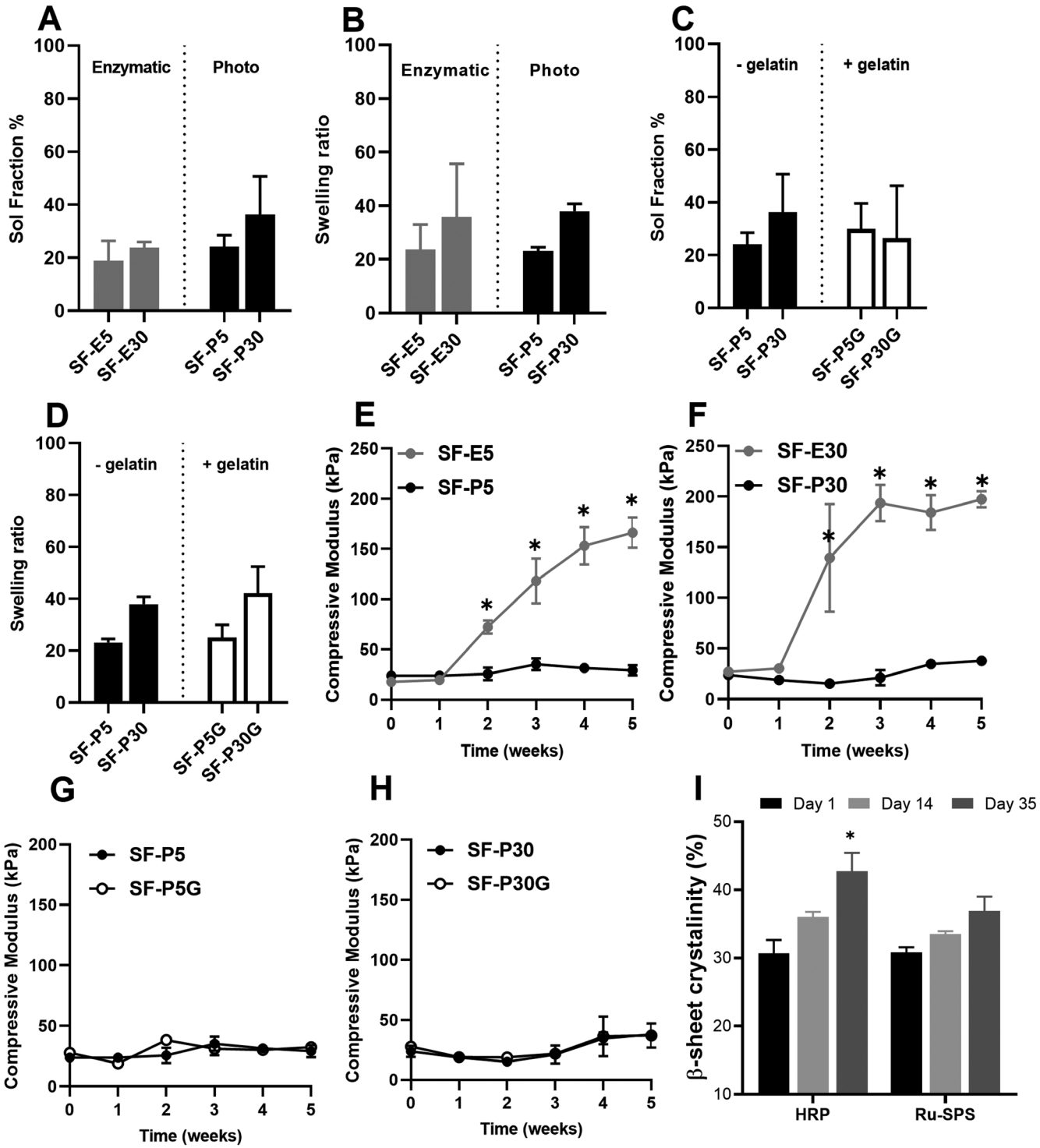

Figure 2. Silk fibroin hydrogels characterization. A) Sol fraction (%) and B) mass swelling ratio of hydrogels fabricated from high (SF-E5, SF-P5) or low (SF-E30, SF-P30) molecular weight silk fibroin using enzymatic (SF-E5, SF-E30) or photocrosslinking (SF-P5, SF-P30) reactions; C) Sol fraction (%) and D) mass swelling ratio of photocrosslinked hydrogels with (SF-P5G, SF-P30G) or without (SF-P5, SF-P30) the addition of gelatin. E,F) Compressive modulus of hydrogels fabricated using enzymatic or photocrosslinking reactions using E) high molecular weight (SF-E5 vs SF-P5) or F) low molecular weight (SF-E30 vs SF-P30) silk fibroin. G,H) Compressive modulus of photocrosslinked hydrogels with or without gelatin fabricated from G) high molecular weight (SF-P5 vs SF-P5G) or H) low molecular weight (SF-P30 vs SF-P30G) silk fibroin. * indicates $p < 0.05$ compared to relative to the counterpart condition at each time point; I) β-sheet crystallinity (%) at 1, 14, and 35 days post-crosslinking as determined by Fourier self-deconvolution of amide I bands (1585–1710 cm^{-1}). * indicates $p < 0.05$ compared to day 1 within each group. $N = 9$ for all conditions. A–D) One-way ANOVA with Bonferroni's multiple comparisons post hoc tests. E–I) Two-way ANOVA with Bonferroni's multiple comparisons post hoc tests.

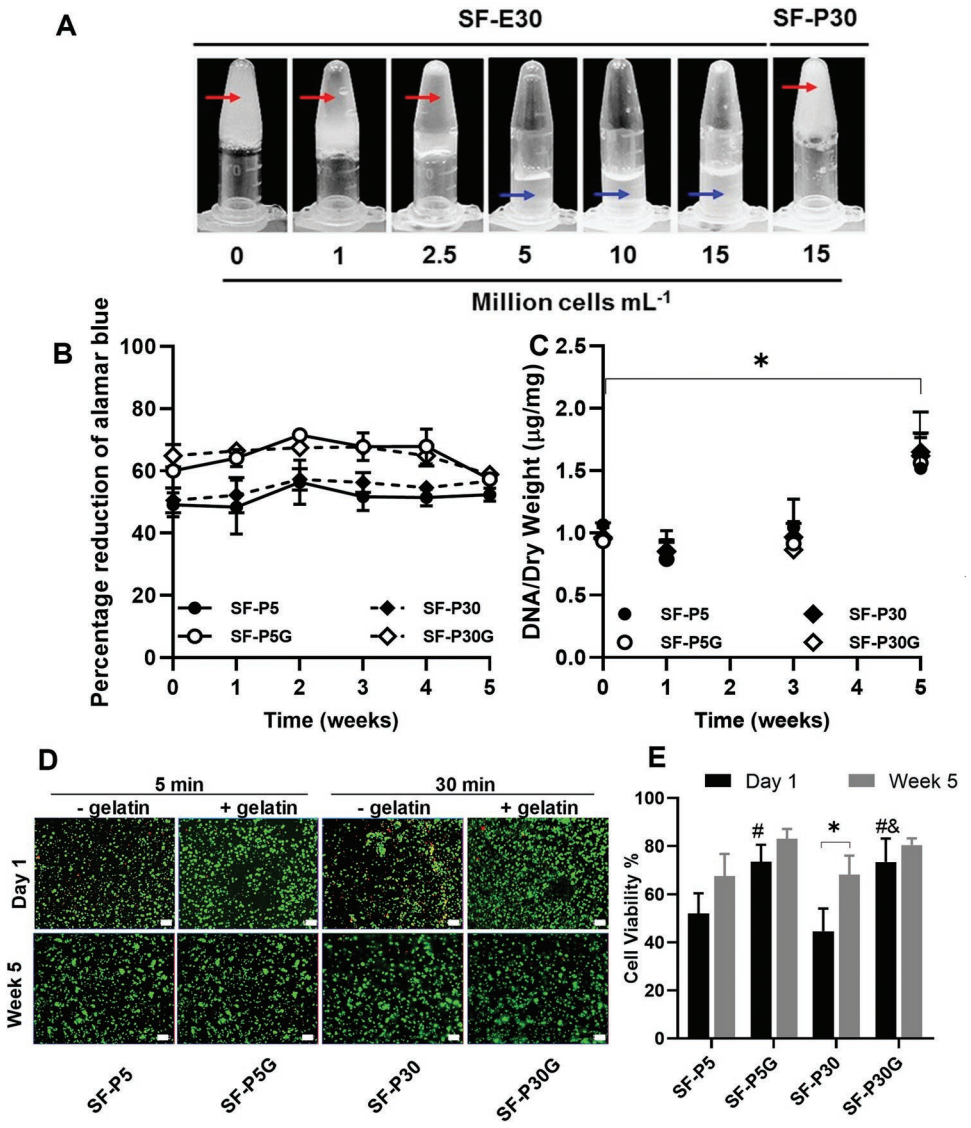

Figure 3. Fabrication of high-density HAC-laden silk fibroin hydrogels for long-term cell culture. A) Macroscopic images of silk fibroin hydrogel formation in the presence of increasing density of HAC (0–15 million cells mL^{-1}) using enzymatic (SF-E30) crosslinking. Photocrosslinking (SF-P30) supported formation of silk fibroin hydrogels of all cell concentration up to 15 million cells mL^{-1}. Red arrows indicate gel formation, blue arrows indicate no gel formation; B–E) Long-term (5 weeks) cell function of HAC encapsulated within photocrosslinked hydrogels fabricated from low (SF-P5, SF-P5G) and high (SF-P30, SF-P30G) molecular weight silk fibroin with (SF-P5G, SF-P30G) or without (SF-P5, SF-P30) the addition of gelatin. B) Cell metabolic activity measured by the reduction of AlamarBlue reagent. C) Total DNA content per dry weight of hydrogel. D) Live/dead images (green = live cells, red = dead cells). E) Cell viability as quantified using live/dead images. Scale bar is 100 µm. * indicates $p < 0.05$ compared to respective day 1 counterparts. # indicates $p < 0.05$ compared to SF-P5 and & indicates $p < 0.05$ compared to SF-P30. $N = 9$ for (B), (C), and (E). Two-way ANOVA with Bonferroni's multiple comparisons post hoc test was used for (B), (C), and (E).

of gelatin (**Figure 4**A and Figure S7, Supporting Information). SF-P5G was the only condition to show a significant increase in the compressive modulus at 1 week ($p < 0.05$), while all the other conditions showed a statistically significant increase at weeks 3 and 5 ($p < 0.0001$). The presence of gelatin had a positive effect on the compressive modulus of both SF-P5G (1.9-fold increase compared to SF-P5, $p < 0.001$) and SF-P30G (1.7-fold increase compared to SF-P30, $p < 0.05$) showing an increase at 3 weeks. Although this trend was also observed in SF-P5G and SF-P30G constructs at 5 weeks, it was only statistically significant in SF-P5G constructs (1.3-fold increase compared to SF-P5, $p < 0.01$). The final compressive modulus after 5 weeks of cell culture ranged from 321.7 ± 26.3 kPa (SF-P30) to 433.5 ± 70.3 kPa (SF-P5G). This increase in compressive modulus over time is correlated with an increase in GAG content, which showed a significant increase over time in all the conditions (Figure 4B). GAG production (GAG/DNA) in all photocrosslinked hydrogels was consistently significantly higher than in the cell pellet control at 3 ($p < 0.0001$) and 5 ($p < 0.0001$) weeks of culture (Figure 4C). The addition of gelatin also enhanced the chondrogenic differentiation capacity as observed by significantly higher GAG/DNA ratio in SF-P5G

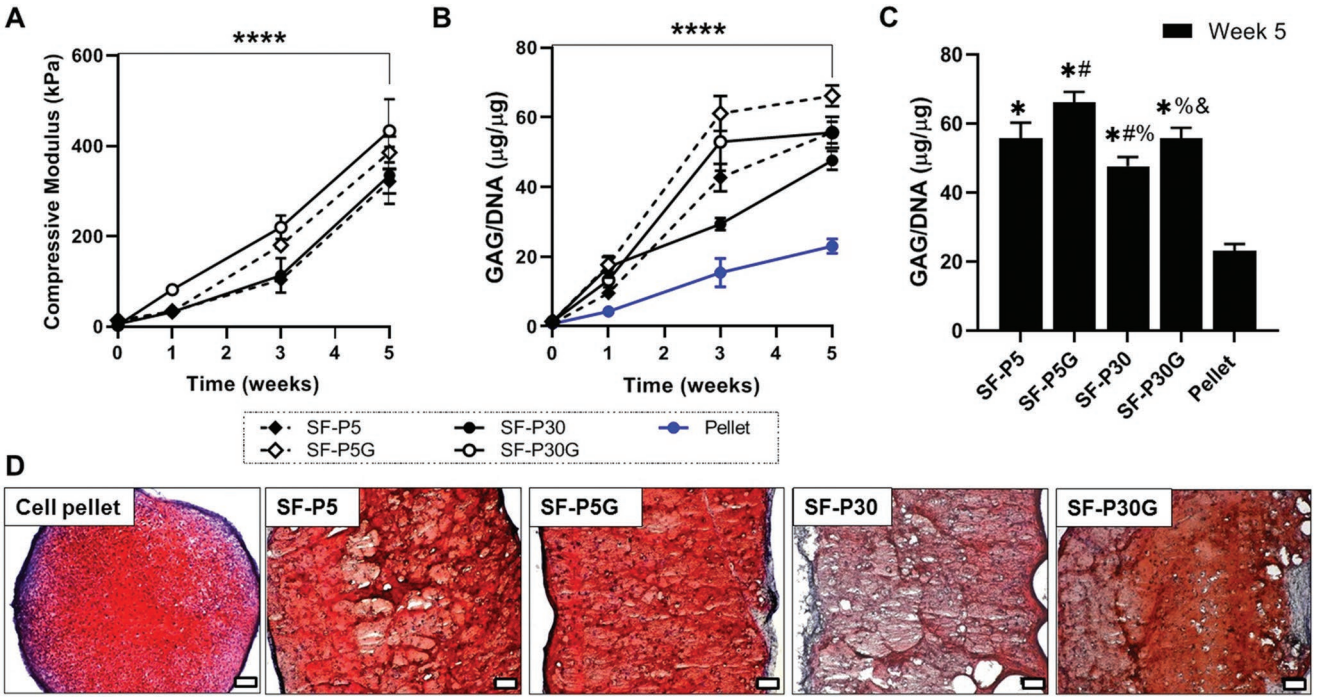

Figure 4. Chondrogenic differentiation of HAC-laden photocrosslinked silk fibroin hydrogels. HACs were encapsulated in photocrosslinked hydrogels fabricated from high (SF-P5, SF-P5G) and low (SF-P30, SF-P30G) molecular weight silk fibroin with (SF-P5G, SF-P30G) or without (SF-P5, SF-P30) the addition of gelatin. A) Compressive modulus of the HAC-laden hydrogels over a 5 weeks culture period, * indicates $p < 0.05$ compared to day 1 for each condition. B) Quantification of GAG/DNA (μg μg^{-1}) content over a 5 week culture period, * indicates $p < 0.05$ compared to day 1 for each condition. C) GAG/DNA (ug ug^{-1}) at the 5 weeks' time point extracted from (B) for better representation of differences between conditions, * indicates $p < 0.05$ compared to pellet, $^{\#}$indicates $p < 0.05$ compared to SF-P5, $^{\%}$indicates $p < 0.05$ compared to SF-P5G, and $^{\&}$indicates $p < 0.05$ compared to SF-P30. D) Visualization of Safranin-O (red)/hematoxylin (dark purple) stains of cryo-sectioned HAC-laden hydrogels after 5 weeks of culture. HAC cell pellet was used as a control. Scale bar = 100 μm. $N = 9$ for (A)–(C). Statistical analysis for (A) and (B) was conducted using two-way ANOVA with Bonferroni's multiple comparisons post hoc test. Statistical analysis for (C) was conducted using one-way ANOVA with Bonferroni's multiple comparisons post hoc test.

and SF-P30G compared to SF-P5 and SF-P30, respectively (**Figure 5**C). The highest GAG/DNA content was in SF-P5G, with 66.2 ± 3.0 μg GAG μg^{-1} DNA, 2.9-fold higher than that in the cell pellet control. Safranin-O staining of GAGs visually confirmed these findings, with SF-P5G showing the most intense red staining, indicating greatest degree of GAG production in the constructs (Figure 4D).

Collagen type I deposition was observed through all the photocrosslinked HAC-laden silk fibroin hydrogels similar to the cell pellet control (Figure 5). Similarly, aggrecan was evenly distributed across all the samples, and no obvious differences were observed between different conditions. In contrast, although collagen type II deposition was observed in all the conditions, it was more evenly distributed and intensely stained in the SF-P5G (Figure 5H) and pellet control (Figure 5B), compared to all the other conditions. Histological analysis of the cell-free control hydrogels is shown in Figure S8 in the Supporting Information. The cytoskeletal structures of the encapsulated HACs were evaluated by F-actin staining (red, Figure 5H,L,P,T). We observed that after 35 days in culture, the HAC embedded in the silk hydrogels presented a round morphology, which is similar to the natural morphology of chondrocytes in native articular cartilage.[32]

These findings were further confirmed by gene expression analysis of chondrogenic markers. There was an increase in collagen types I and II expression in all the conditions over a 5 week culture period (**Figure 6**A,B). Specifically for collagen type II, all photocrosslinked hydrogels had significantly higher collagen type II expression after 5 weeks of culture compared to the positive pellet control (Figure 6B). This result was further reflected in the collagen type II/ I ratio, where all photocrosslinked HAC-laden hydrogels had at least tenfold higher collagen type II/I ratio compared to the pellet control (Figure 6C). Interestingly, there were no significant differences between the samples of different molecular weight or with the presence of gelatin in terms of collagen type I and type II expressions. The effect of gelatin incorporation on chondrogenesis of HAC was however prominent for collagen type X, where both SF-P5G and SF-P30G had higher collagen type X expression compared to SF-P5 and SF-P30, respectively (Figure 6D). Aggrecan expression was not statistically different to the pellet controls at the 5 week time point. A decrease in Sox-9 expression was observed after 1 week of culture in all the photocrosslinked hydrogels, but the overall Sox-9 expression was still significantly higher compared to the pellet control after 5 weeks of culture (Figure 6F).

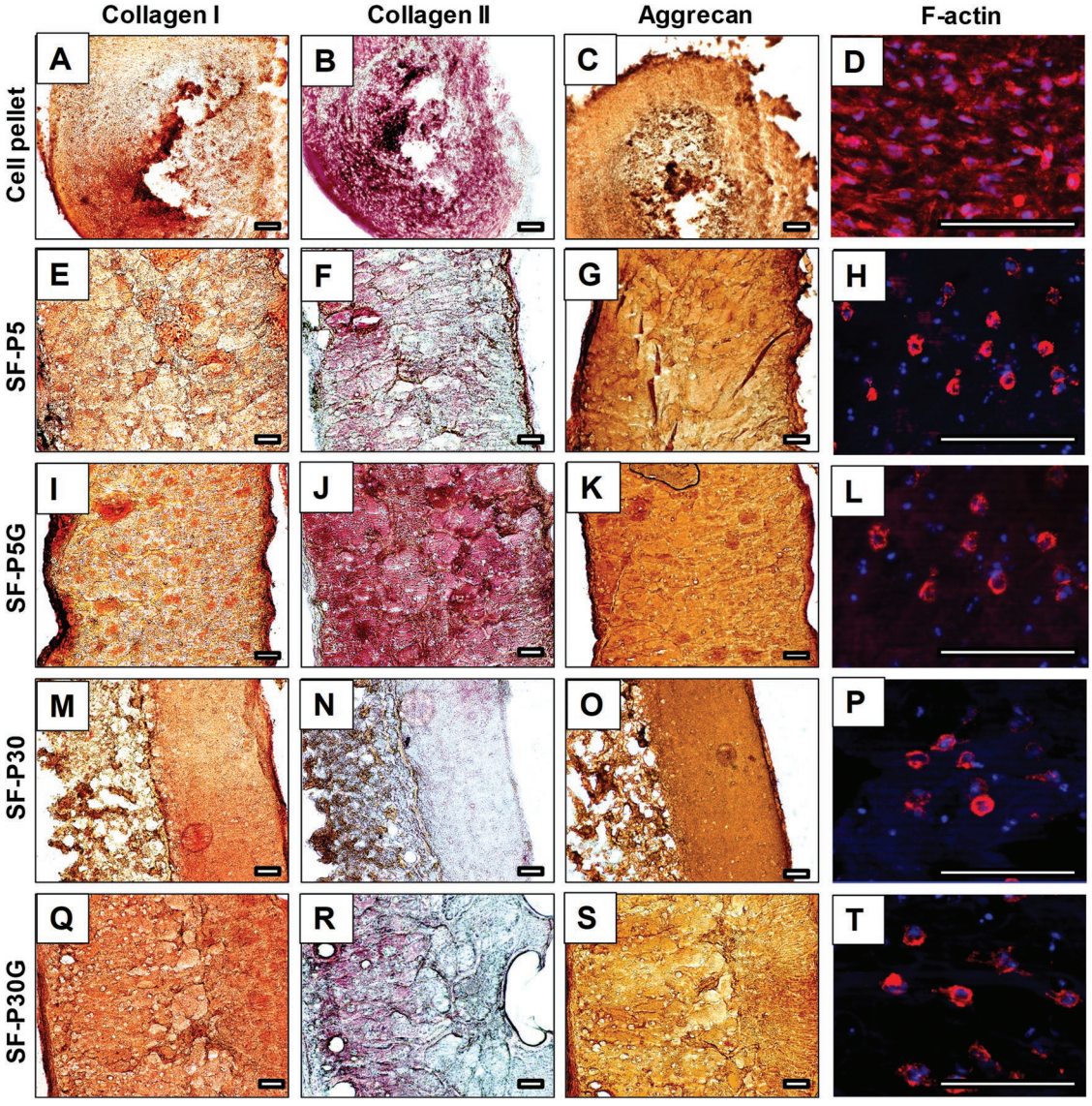

Figure 5. Immunohistochemical analysis of the ECM (collagen I, collagen II, and aggrecan) production of HAC in cryo-sectioned HAC-laden silk fibroin hydrogels cultured for 5 weeks and cytoskeletal structure of HAC in cryo-sectioned HAC-laden silk fibroin hydrogels cultured for 5 weeks. A–D) HAC pellet positive control constructs. E–L) Photocrosslinked hydrogels fabricated from high molecular weight silk without gelatin (SF-P5, E-H) or with gelatin (SF-P5G, I-L). M–T) Photocrosslinked hydrogels fabricated from low molecular weight silk fibroin M–P) without gelatin (SF-P30) or Q–T) with gelatin (SF-P30G). Scale bar = 100 µm. Orange staining indicates collagen I or aggrecan deposition in columns 1 and 3, while Fuschia staining indicated collagen II deposition in column 2. In column 4, Red staining is F-actin and blue staining is 4′,6-diamidino-2-phenylindole. Scale bar is 100 µm.

3.4. 3D Biofabrication of Complex Cell-Laden Silk Fibroin Hydrogels Using Visible Light-Mediated Photocrosslinking

The utility of the photocrosslinking approach in biofabrication of silk hydrogels with complex architectures was investigated and compared to the enzymatic crosslinking approach. First, sacrificial templates made of Pluronic F-127 were extruded followed by extrusion of the silk hydrogel solution into the sacrificial template (Figure S1, Supporting Information). The Pluronic F-127 was leached away post-crosslinking, leaving intact silk hydrogels of various patterns, orientations, and architectures depending on the initial template design. Enzymatic crosslinking was not compatible with the 3D biofabrication approach, as the silk hydrogels had no structural integrity and collapsed post-crosslinking (**Figure 7**A,C). In contrast, the photocrosslinking approach supported rapid 3D sacrificial biofabrication of silk fibroin hydrogels, where constructs with ordered architecture (pore size = 0.75 mm) were successfully fabricated (Figure 7D).

This rapid photomediated di-tyrosine crosslinking of silk fibroin hydrogels was further exploited to fabricate constructs of various sizes with different internal pore sizes (**Figure 8**A–C). The pore sizes could be tailored between 500 and 1000 µm depending on the design of the sacrificial Pluronic F-127

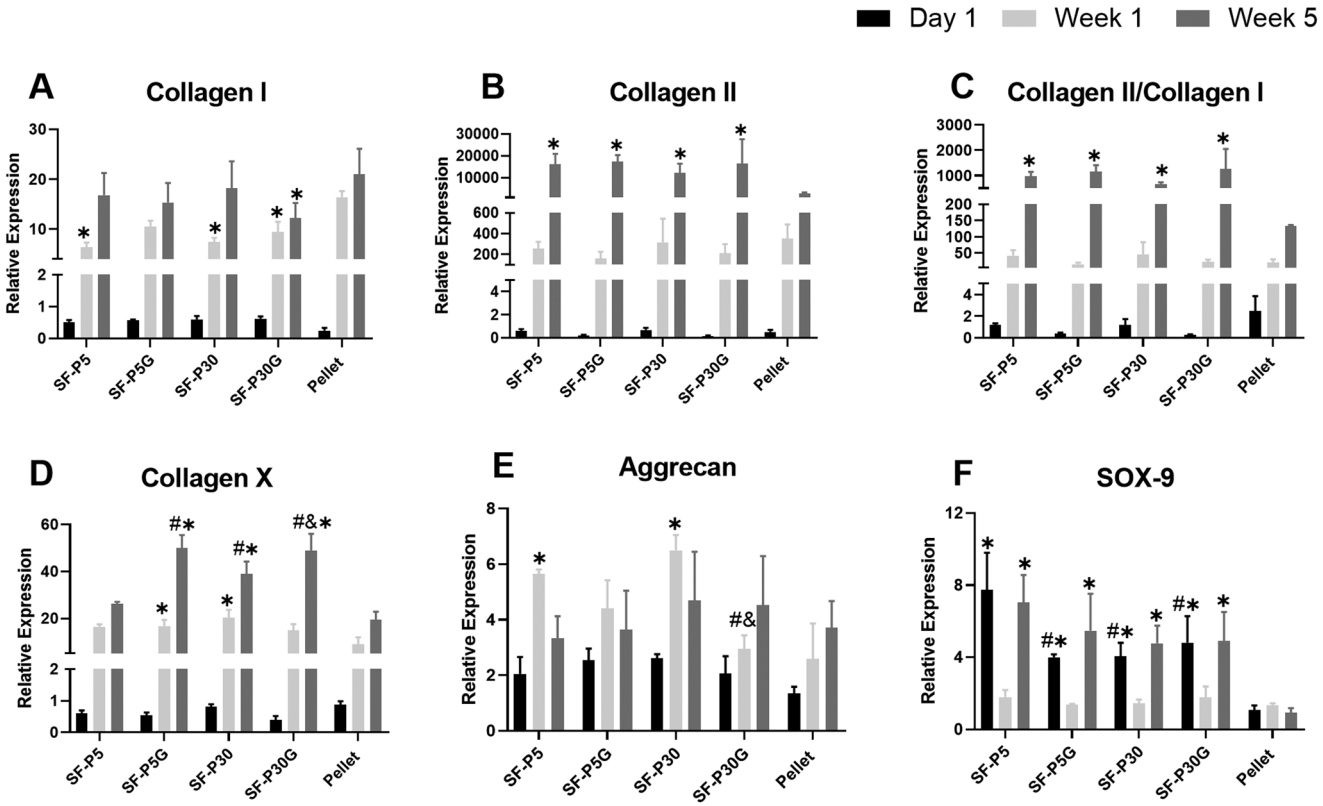

Figure 6. Relative gene expression in HAC encapsulated in silk fibroin hydrogels. HAC were encapsulated in photocrosslinked hydrogels fabricated from high (SF-P5, SF-P5G) or low (SF-P30, SF-P30G) silk fibroin with (SF-P5G, SF-P30G) or without (SF-P5, SF-P30) gelatin. Gene expression was analyzed at 1 day, 1 week, and 5 weeks of culture in chondrogenic media. Relative expression of A) collagen type I, B) collagen type II, C) collagen type II/I ratio, D) collagen type X, E) aggrecan, and F) Sox-9. HAC pellets were used as a positive control. * denotes statistical significance ($p < 0.05$) compared to the pellet control; #indicates statistical significance ($p < 0.05$) compared to SF-P5; &indicates statistical significance ($p < 0.05$) compared to SF-P30. N = 9 for all conditions. Two-way ANOVA with Bonferroni's multiple comparisons post hoc test was used to analyze all the data.

template (Figures S2 and S3, Supporting Information). The constructs showed good shape fidelity and stability in both top (Figure 8A–C) and side view (Figure S2, Supporting Information). Furthermore, silk fibroin hydrogels of different thickness (1–10 mm depending on the number of extruded Pluronic F-127 layers) and shape such as hollow cylindrical conduits with different inner channel designs were easily fabricated (Figure S9, Supporting Information). By changing the design of the sacrificial template (0°–45° to 135°–90° orientation), hydrogels with complex interconnected channels were easily fabricated (Figure 8D–F). Moreover, sophisticated silk fibroin hydrogels were successfully printed, where fibers of different diameters (40–120 µm, Figure 8F, white arrows) were not only localized at different angles (Figure 8F), but were also spaced at different distances (Figure 8G–I, red arrows). Specifically, the silk fibroin fibers were spaced at 100 µm (Figure 8G), 250 µm (Figure 8H), and 400 µm (Figure 8I), all within one construct, highlighting the capacity to fabricate intricate, complex, and graduated silk fibroin hydrogels using the combination of the photocrosslinking reaction with sacrificial 3D biofabrication.

In order to evaluate the cyto-compatibility of this biofabrication approach, silk hydrogel solution containing HAC was extruded onto a simple Pluronic F-127 lattice template (0°–90° orientation, Figure 8J), followed by visible light photocrosslinking. Upon removal of the sacrificial template, the cell-laden silk hydrogels not only retained the structural integrity and shape, but also supported high cell viability (72.38 ± 1.32%) and homogenous cell distribution (Figure 8K). Similar to the cast photocrosslinked silk hydrogels, HACs encapsulated in the 3D biofabricated silk hydrogels were able to secrete ECM, including GAGs, collagen type I, collagen type II, and aggrecan after 5 weeks of culture in chondrogenic media (Figure 8L and Figure S10, Supporting Information). The GAG and protein deposition were homogenously distributed throughout the constructs, further indicating that the sacrificial 3D biofabrication process did not affect the HAC functionality.

4. Discussion

Di-tyrosine crosslinking of silk fibroin has been developed in pursuit of fabrication of elastomeric hydrogels that do not rely on structural transformation of silk fibroin to β-sheets used in conventional silk fibroin hydrogel fabrication approaches.[3b] Although the enzymatic (HRP/H_2O_2) crosslinking system is best described toward this goal, it requires relatively long gelation times and these constructs have been shown to undergo

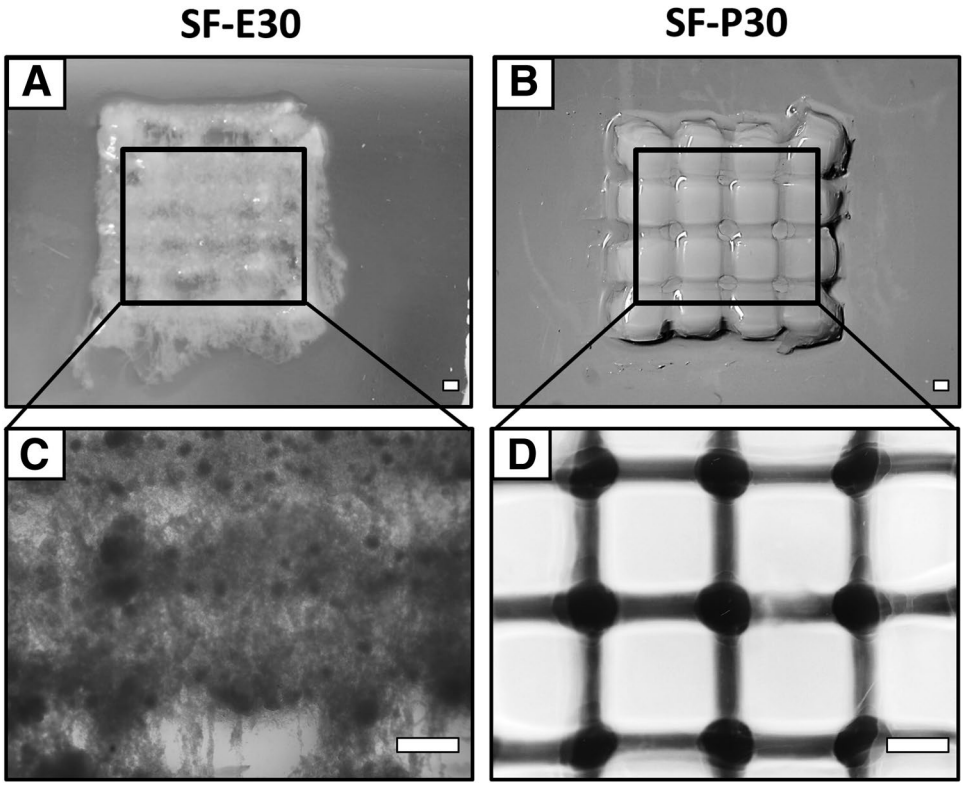

Figure 7. 3D biofabrication of silk fibroin hydrogels using Pluronic F-127 sacrificial templating (12 × 12 mm, 0–90° to 0-90° orientation, seven layers). A,B) Macroscopic images of A) enzymatic or B) photocrosslinked hydrogels. C,D) Microscopic images of C) enzymatic or D) photocrosslinked hydrogels. The samples were fabricated using low molecular weight silk (SF-E30, SF-P30). Scale bar = 1 mm.

spontaneous transition to stiff β-sheet-rich constructs over time.[4] To circumvent these issues and generate stable, elastomeric silk fibroin hydrogels compatible with high density cell encapsulation, di-tyrosine crosslinking using Ru/SPS was utilized to crosslink silk fibroin in less than 1 min. In fact, our photorheological data showed that 5 s of light irradiation was sufficient to facilitate the sol–gel transition process, but a minimum of 10 s was required to achieve the minimal sol fraction (Figure S5C, Supporting Information). In comparison to the enzymatic crosslinking system, although we observed sol–gel transition after 25 min, these gels were incompletely crosslinked where a total of 90 min was required for the sol fraction value to plateau (Figure S5D, Supporting Information). The crosslinking efficiency (as indicated by sol fraction value and swelling ratio) was however similar in the two crosslinking systems once complete crosslinking was achieved, and was not affected by the molecular weight of silk fibroin suggesting that the radicals responsible for crosslinking could effectively propagate through both high and low molecular weight polymer networks.

Hydrogels generated by both the enzymatic and the photocrosslinking approaches had similar mechanical stiffness and low β-sheet content immediately post-fabrication. However, while the enzymatically crosslinked hydrogels underwent a structural transformation to high β-sheet and showed gradual mechanical stiffening over time (similar to previous reports[4]), this trend was not observed in photocrosslinked hydrogels. Considering the two crosslinking approaches are expected to follow the same crosslinking pathway and similarities in the physico-chemical properties immediately post-fabrication, this was a surprising finding. We hypothesize that the cause of this dissimilarity is heterogeneity in the hydrogels network formation at the microstructural level caused by differences in the ability of HRP (Mw = 44 000 Da) and Ru (Mw = 750 Da) to propagate through the system. The much smaller ruthenium may easily propagate through the system, allowing for more homogenous crosslinking which then prevents structural transformation of silk fibroin to β-sheets. Hydrogel stiffness is well established to affect cellular activity, including cell differentiation,[33] as well as oxygen/nutrient transport, hydrophilicity, and availability of cell binding sites[33,34] within the hydrogel network. Within this context, the photocrosslinking reaction offers a rapid pathway to fabricate silk hydrogels with controllable and predictable mechanical properties, with potential to be tailored for a range of regenerative medicine applications. The difference in mechanical stability between the enzymatically and photocrosslinked systems might also result in different degradation profiles in vivo, which might affect overall tissue integration and host response. While it is of interest to explore the in vivo degradation behavior of these di-tyrosine crosslinked silk hydrogels, and particularly comparing between the HRP/H_2O_2 and Ru/SPS systems, this is outside the scope of the current paper and will be pursued in future studies.

Another major advantage of the photocrosslinking system presented in this work is the ability to encapsulate cells. Although the use of the ruthenium system to photocrosslink

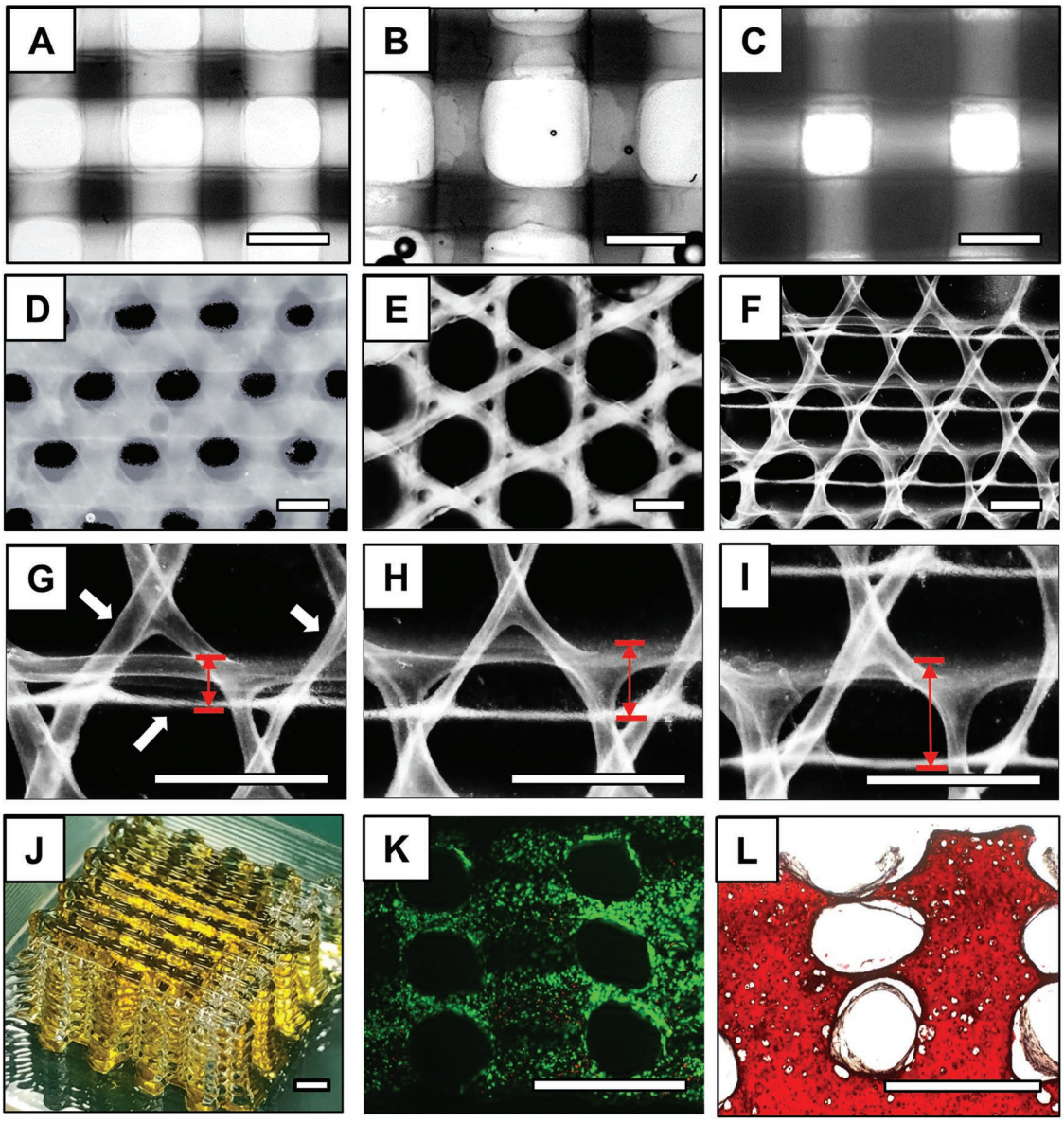

Figure 8. Microscopic images of a range of 3D biofabricated photocrosslinked silk fibroin hydrogel architectures prepared using Pluronic F-127 sacrificial templates. A–F) Microscopic A–C) top-view images of 0°–90° orientated channeled networks (black) within silk fibroin hydrogels (white) with varying channel sizes, including A) 0.25 mm, B) 0.5 mm, and C) 1 mm. D–F) Microscopic top-view images of 0°–45° to 135°–90° orientation channeled networks (black) within silk fibroin hydrogels (white) with varying Pluronic F-127 filament spacing, including D) 0.5 mm and E) 0.2 mm. G–I) Zoomed-in top-view images of (F), showing hydrogel features of varying sizes within a single construct, with silk fibroin filaments ranging from 40 to 120 µm (G, white arrows) and filament spacing (red arrows) of G) 100 µm, H) 250 µm, and I) 400 µm. J–L) 3D biofabrication of HAC-laden silk hydrogels using SF-P5G: J) Macroscopic image of silk fibroin hydrogel containing HAC (yellow) extruded onto a Pluronic F-127 sacrificial template (white/clear) using a dual extrusion 3D biofabrication process. K) Live/dead images at day 1 (green-live, red-dead). L) Safranin-O staining (red) at week 5. Scale bar = 1 mm.

silk hydrogels has been previously demonstrated, these studies did not involve cell encapsulation nor evaluate long-term cell functionality.[19a,b] In this study, it was showed the photocrosslinking system supported encapsulation of cells at high densities (up to 15 million cells mL^{-1}), which has not been achieved with the enzymatic crosslinking system to date.[13b] In fact, the enzymatic crosslinking mechanism only allowed hydrogel formation in the presence of up to 2.5 million cells mL^{-1}. This difference between the two crosslinking systems is likely due to the availability of radicals during the reaction. While the presence of cells is likely to be quenching radicals in both systems,[34] the photoredox reaction has been reported to undergo a self-recycling mechanism, resulting in a more sustained radical generation rate leading to a lower susceptibility of radicals quenching.[19c,21] Cell encapsulation at high density is crucial in many regenerative medicine applications, including in cartilage tissue engineering where high cell concentration is required to maximize

the total amount of tissue formed.[35] Moreover, cell–cell communication is essential for chondrogenesis, as blocking gap junction-mediated cell interactions have been shown to compromise cell differentiation and subsequent tissue formation.[36] Erickson et al. previously showed that in hyaluronan hydrogels, high cell density is required to facilitate efficient paracrine signaling which is crucial for chondrogenesis.[37] The Ru/SPS photocrosslinked silk hydrogels presented in this study not only supported HAC encapsulation up to 15 million cells mL^{-1} at high cell viability but also supported subsequent efficient chondrogenic differentiation and tissue formation. In order to validate silk hydrogels as a biomaterial for cartilage tissue engineering, cell activity in the silk hydrogels was compared to that in the HAC pellet culture, a well-known autograft used in the clinic.[38] GAG secretion was higher in cells encapsulated in silk hydrogels compared to those in the pellet control. Silk hydrogels supported secretion of type II collagen and aggrecan, key components of the healthy cartilage ECM,[31] and higher collagen II/collagen I expression ratios, demonstrating the potential of these constructs for clinical repair of cartilage. The highly hydrated and permissive microenvironment of the silk hydrogels can facilitate sufficient oxygen and nutrient transportation, which is essential to support cell functionality.[39] In addition, the mechanical properties of the silk hydrogel obtained in this study are around 10–15 kPa, which has been previously documented to promote HAC proliferation and GAG deposition.[40]

The rapid photocrosslinking strategy described in this work presents additional advantages in 3D biofabrication. One key example demonstrated in this current study is the rapid stabilization of the silk bioink mediated by visible light exposure, permitting the creation of complex porous architectures via extrusion printing within a sacrificial template. It is to be highlighted that the silk bioink in this study has not undergone any lengthy modification process to graft photolabile groups onto the protein, nor require addition of rheological modifiers as per the literature.[22–24] By tuning the resolution and design of the sacrificial Pluronic F-127 sacrificial template, silk fibroin filaments of high resolution (40 μm) were printed, superior to previously reported studies using this sacrificial approach and gelatin-based inks.[41] Although previous studies have shown the use of the same ruthenium-based photocrosslinking system for 3D printing of silk constructs using multiphoton lithography, these studies did not include cells during the printing process.[19a,b] In this study, we demonstrated that the visible light-initiated photoredox platform not only allows formation of sophisticated, ordered, and graduated constructs but also supported encapsulation of cells at high densities with long-term survival and function following biofabrication. We believe that this system holds great potential for complex and free-form architectures that can be obtained through further development of this photoresponsive silk bioink, especially using light-based biofabrication technologies such as projection lithography,[25,42] or even via recently developed fast tomographic volumetric bioprinting technologies.[43] Finally, future studies will explore in vivo responses to this new hydrogel system and in particular investigate the beta-sheet transformation and degradation mechanisms of this new class of silk hydrogel post-implantation.

5. Conclusion

This study demonstrates a novel, visible light-mediated photocrosslinking approach for fabrication of silk hydrogels through di-tyrosine crosslinking. This approach generates robust and stable hydrogels that do not undergo spontaneous transition to stiff β-sheet-rich silk constructs, and support cell encapsulation at very high densities, allowing robust formation of cartilage tissue in vitro. The system is compatible with biofabrication approaches, allowing formation of complex constructs with ordered architectures, and demonstrating the utility of photocrosslinked silk hydrogels in tissue engineering and regenerative medicine applications.

Supporting Information

Supporting Information is available from the Wiley Online Library or from the author.

Acknowledgements

X.C. acknowledges the funding by University of Otago Health Science Postdoctoral Fellowship and New Zealand Health Research Council (Explorer Grant – 19/779). K.L. acknowledges funding by Health Research Council of New Zealand (Emerging Researcher First Grant – 15/483, Sir Charles Hercus Health Research Fellowship – 19/135) and Royal Society of New Zealand (Marsden Fast Start – MFP-UOO1826). J.R.-K. acknowledges funding support from the Australian Research Council (DP150104242) and the National Heart Foundation of Australia Australian Future Leader Fellowship (101896). S.G.W. and J.R.-K. received funding from the National Health and Medical Research Council (APP1162969). T.W. acknowledges funding from Royal Society of New Zealand (Rutherford Discovery Fellowship – RDF-UOO1204). The authors thank Associate Professor Ken Morison from the University of Canterbury for helping them with the rheology tests.

Conflict of Interest

The authors declare no conflict of interest.

Keywords

biofabrication, cartilage, photo-polymerization, silk fibroin, visible light

Received: November 22, 2019
Revised: December 12, 2019
Published online: January 15, 2020

[1] C. Holland, K. Numata, J. Rnjak-Kovacina, F. P. Seib, *Adv. Healthcare Mater.* **2019**, *8*, 1800465.
[2] H. Tao, D. L. Kaplan, F. G. Omenetto, *Adv. Mater.* **2012**, *24*, 2824.
[3] a) K. H. Bae, L.-S. Wang, M. Kurisawa, *J. Mater. Chem. B* **2013**, *1*, 5371; b) B. P. Partlow, C. W. Hanna, J. Rnjak-Kovacina, J. E. Moreau, M. B. Applegate, K. A. Burke, B. Marelli, A. N. Mitropoulos, F. G. Omenetto, D. L. Kaplan, *Adv. Funct. Mater.* **2014**, *24*, 4615; c) X. Leng, B. Liu, B. Su, M. Liang, L. Shi, S. Li, S. Qu, X. Fu, Y. Liu, M. Yao, D. L. Kaplan, Y. Wang, X. Wang, *J. Tissue Eng. Regener. Med.* **2017**, *11*, 822; d) Y. Cao, B. Wang, *Int. J. Mol. Sci.* **2009**, *10*, 1514.

[4] N. R. Raia, B. P. Partlow, M. McGill, E. P. Kimmerling, C. E. Ghezzi, D. L. Kaplan, *Biomaterials* **2017**, *131*, 58.
[5] a) F. G. Omenetto, D. L. Kaplan, *Science* **2010**, *329*, 528; b) E. M. Pritchard, D. L. Kaplan, *Expert Opin. Drug Delivery* **2011**, *8*, 797.
[6] L. Meinel, S. Hofmann, V. Karageorgiou, C. Kirker-Head, J. McCool, G. Gronowicz, L. Zichner, R. Langer, G. Vunjak-Novakovic, D. L. Kaplan, *Biomaterials* **2005**, *26*, 147.
[7] X. Wang, J. A. Kluge, G. G. Leisk, D. L. Kaplan, *Biomaterials* **2008**, *29*, 1054.
[8] U. J. Kim, J. Park, C. Li, H. J. Jin, R. Valluzzi, D. L. Kaplan, *Biomacromolecules* **2004**, *5*, 786.
[9] T. Yucel, P. Cebe, D. L. Kaplan, *Biophys. J.* **2009**, *97*, 2044.
[10] G. G. Leisk, T. J. Lo, T. Yucel, Q. Lu, D. L. Kaplan, *Adv. Mater.* **2010**, *22*, 711.
[11] G.-D. Kang, J.-H. Nahm, J.-S. Park, J.-Y. Moon, C.-S. Cho, J.-H. Yeo, *Macromol. Rapid Commun.* **2000**, *21*, 788.
[12] A. R. Murphy, D. L. Kaplan, *J. Mater. Chem.* **2009**, *19*, 6443.
[13] a) M. R. Carvalho, F. R. Maia, S. Vieira, R. L. Reis, J. M. Oliveira, *Global Challenges* **2018**, *2*, 1700100; b) V. P. Ribeiro, J. Silva-Correia, C. Gonçalves, S. Pina, H. Radhouani, T. Montonen, J. Hyttinen, A. Roy, A. L. Oliveira, R. L. Reis, J. M. Oliveira, *PLoS One* **2018**, *13*, e0194441; c) L.-P. Yan, J. Silva-Correia, V. P. Ribeiro, V. Miranda-Gonçalves, C. Correia, A. da Silva Morais, R. A. Sousa, R. M. Reis, A. L. Oliveira, J. M. Oliveira, R. L. Reis, *Sci. Rep.* **2016**, *6*, 31037; d) J. J. Roberts, P. Naudiyal, K. S. Lim, L. A. Poole-Warren, P. J. Martens, *Biomater. Res.* **2016**, *20*, 30;
[14] W. Hu, Z. Wang, Y. Xiao, S. Zhang, J. Wang, *Biomater. Sci.* **2019**, *7*, 843.
[15] a) M. Ott, V. Gogvadze, S. Orrenius, B. Zhivotovsky, *Apoptosis* **2007**, *12*, 913; b) C. S. W. A. J. Dahm-Daphi, *Int. J. Radiat. Biol.* **2000**, *76*, 67.
[16] M. B. Applegate, B. P. Partlow, J. Coburn, B. Marelli, C. Pirie, R. Pineda, D. L. Kaplan, F. G. Omenetto, *Adv. Mater.* **2016**, *28*, 2417.
[17] Y.-L. Sun, Q. Li, S.-M. Sun, J.-C. Huang, B.-Y. Zheng, Q.-D. Chen, Z.-Z. Shao, H.-B. Sun, *Nat. Commun.* **2015**, *6*, 8612.
[18] B. P. Partlow, M. B. Applegate, F. G. Omenetto, D. L. Kaplan, *ACS Biomater. Sci. Eng.* **2016**, *2*, 2108.
[19] a) M. B. Dickerson, P. B. Dennis, V. P. Tondiglia, L. J. Nadeau, K. M. Singh, L. F. Drummy, B. P. Partlow, D. P. Brown, F. G. Omenetto, D. L. Kaplan, R. R. Naik, *ACS Biomater. Sci. Eng.* **2017**, *3*, 2064; b) J. L. Whittaker, N. R. Choudhury, N. K. Dutta, A. Zannettino, *J. Mater. Chem. B* **2014**, *2*, 6259; c) D. A. Fancy, T. Kodadek, *Proc. Natl. Acad. Sci. U. S. A.* **1999**, *96*, 6020.
[20] a) L. Sando, S. Danon, A. G. Brownlee, R. J. McCulloch, J. A. M. Ramshaw, C. M. Elvin, J. A. Werkmeister, *J. Tissue Eng. Regener. Med.* **2011**, *5*, 337; b) J. W. Bjork, S. L. Johnson, R. T. Tranquillo, *Biomaterials* **2011**, *32*, 2479; c) Z. H. Syedain, J. Bjork, L. Sando, R. T. Tranquillo, *Biomaterials* **2009**, *30*, 6695; d) C. M. Elvin, T. Vuocolo, A. G. Brownlee, L. Sando, M. G. Huson, N. E. Liyou, P. R. Stockwell, R. E. Lyons, M. Kim, G. A. Edwards, G. Johnson, G. A. McFarland, J. A. M. Ramshaw, J. A. Werkmeister, *Biomaterials* **2010**, *31*, 8323.
[21] K. S. Lim, B. S. Schon, N. V. Mekhileri, G. C. J. Brown, C. M. Chia, S. Prabakar, G. J. Hooper, T. B. F. Woodfield, *ACS Biomater. Sci. Eng.* **2016**, *2*, 1752.
[22] S. Das, F. Pati, Y.-J. Choi, G. Rijal, J.-H. Shim, S. W. Kim, A. R. Ray, D.-W. Cho, S. Ghosh, *Acta Biomater.* **2015**, *11*, 233.
[23] M. J. Rodriguez, J. Brown, J. Giordano, S. J. Lin, F. G. Omenetto, D. L. Kaplan, *Biomaterials* **2017**, *117*, 105.
[24] Z. Zheng, J. Wu, M. Liu, H. Wang, C. Li, M. J. Rodriguez, G. Li, X. Wang, D. L. Kaplan, *Adv. Healthcare Mater.* **2018**, *7*, 1701026.
[25] S. H. Kim, Y. K. Yeon, J. M. Lee, J. R. Chao, Y. J. Lee, Y. B. Seo, M. T. Sultan, O. J. Lee, J. S. Lee, S.-I. Yoon, I.-S. Hong, G. Khang, S. J. Lee, J. J. Yoo, C. H. Park, *Nat. Commun.* **2018**, *9*, 1620.
[26] D. N. Rockwood, R. C. Preda, T. Yucel, X. Q. Wang, M. L. Lovett, D. L. Kaplan, *Nat. Protoc.* **2011**, *6*, 1612.
[27] J. Rnjak-Kovacina, L. S. Wray, K. A. Burke, T. Torregrosa, J. M. Golinski, W. W. Huang, D. L. Kaplan, *ACS Biomater. Sci. Eng.* **2015**, *1*, 260.
[28] E. C. Filipe, M. Santos, J. Hung, B. S. L. Lee, N. Yang, A. H. P. Chan, M. K. C. Ng, J. Rnjak-Kovacina, S. G. Wise, *JACC: Basic Transl. Sci.* **2018**, *3*, 38.
[29] B. S. Schon, K. Schrobback, M. van der Ven, S. Stroebel, G. J. Hooper, T. B. Woodfield, *Cell Tissue Res.* **2012**, *347*, 629.
[30] Y. Shachaf, M. Gonen-Wadmany, D. Seliktar, *Biomaterials* **2010**, *31*, 2836.
[31] a) D. Eyre, *Arthritis Res.* **2002**, *4*, 30; b) A. R. Klatt, B. Paul-Klausch, G. Klinger, G. Kuhn, J. H. Renno, M. Banerjee, G. Malchau, K. Wielckens, *J. Orthop. Res.* **2009**, *27*, 65; c) C. Kiani, L. Chen, Y. J. Wu, A. J. Yee, B. B. Yang, *Cell Res.* **2002**, *12*, 19; d) P. J. Roughley, J. S. Mort, *J. Exp. Orthop.* **2014**, *1*, 8.
[32] E. Langelier, R. Suetterlin, C. D. Hoemann, U. Aebi, M. D. Buschmann, *J. Histochem. Cytochem.* **2000**, *48*, 1307.
[33] a) K. M. Schultz, K. A. Kyburz, K. S. Anseth, *Proc. Natl. Acad. Sci. U. S. A.* **2015**, *112*, E3757; b) M. Guvendiren, J. A. Burdick, *Nat. Commun.* **2012**, *3*, 792.
[34] a) J. Li, Y. Wang, S.-L. Chiu, H. T. Cline, *Front. Neural Circuits* **2010**, *4*, 6; b) K. Honke, N. Kotani, *Sensors* **2012**, *12*, 16037.
[35] G. C. J. Brown, K. S. Lim, B. L. Farrugia, G. J. Hooper, T. B. F. Woodfield, *Macromol. Biosci.* **2017**, *17*, 1700158.
[36] K. Schrobback, T. J. Klein. T. B. F. Woodfield, *Tissue Eng., Part A* **2015**, *21*, 1785.
[37] I. E. Erickson, S. R. Kestle, K. H. Zellars, M. J. Farrell, M. Kim, J. A. Burdick, R. L. Mauck, *Acta Biomater.* **2012**, *8*, 3027.
[38] a) B. D. Markway, H. Cho, B. Johnstone, *Arthritis Res. Ther.* **2013**, *15*, R92; b) B. S. Schon, K. Schrobback, M. van der Ven, S. Stroebel, G. J. Hooper, T. B. F. Woodfield, *Cell Tissue Res.* **2012**, *347*, 629.
[39] a) X. Cui, J. Tang, Y. Hartanto, J. Zhang, J. Bi, S. Dai, S. Z. Qiao, K. Cheng, H. Zhang, *ACS Appl. Mater. Interfaces* **2018**, *10*, 37783; b) X. Cui, Y. Hartanto, C. Wu, J. Bi, S. Dai, H. Zhang, *J. Biomed. Mater. Res., Part A* **2018**, *106*, 2899.
[40] a) T. Wang, J. H. Lai, L.-H. Han, X. Tong, F. Yang, *J. Mater. Chem. B* **2016**, *4*, 7641; b) T. Wang, J. H. Lai, F. Yang, *Tissue Eng., Part A* **2016**, *22*, 1348.
[41] R. Levato, W. R. Webb, I. A. Otto, A. Mensinga, Y. Zhang, M. van Rijen, R. van Weeren, I. M. Khan, J. Malda, *Acta Biomater.* **2017**, *61*, 41.
[42] K. S. Lim, R. Levato, P. F. Costa, M. D. Castilho, C. R. Alcala-Orozco, K. M. A. van Dorenmalen, F. P. W. Melchels, D. Gawlitta, G. J. Hooper, J. Malda, T. B. F. Woodfield, *Biofabrication* **2018**, *10*, 034101.
[43] P. N. Bernal, P. Delrot, D. Loterie, Y. Li, J. Malda, C. Moser, R. Levato, *Adv. Mater.* **2019**, *31*, 1904209.